NASA TECHNICAL MEMORANDUM

NASA TM X-2028

NASA TM X-2028

COOLANT PRESSURE AND FLOW DISTRIBUTION THROUGH AN AIR-COOLED VANE FOR A HIGH-TEMPERATURE GAS TURBINE

by John S. Clark, Hadley T. Richards, David J. Poferl, and John N. B. Livingood

Lewis Research Center
Cleveland, Ohio 44135

NATIONAL AERONAUTICS AND SPACE ADMINISTRATION • WASHINGTON, D. C. • JUNE 1970

1. Report No. NASA TM X-2028	2. Government Accession No.	3. Recipient's Catalog No.
4. Title and Subtitle COOLANT PRESSURE AND FLOW DISTRIBUTION THROUGH AN AIR-COOLED VANE FOR A HIGH-TEMPERATURE GAS TURBINE		5. Report Date June 1970 6. Performing Organization Code
7. Author(s) John S. Clark, Hadley T. Richards, David J. Poferl, and John N. B. Livingood		8. Performing Organization Report No. E-5558
9. Performing Organization Name and Address Lewis Research Center National Aeronautics and Space Administration Cleveland, Ohio 44135		10. Work Unit No. 720-03 11. Contract or Grant No. 13. Type of Report and Period Covered Technical Memorandum
12. Sponsoring Agency Name and Address National Aeronautics and Space Administration Washington, D.C. 20546		14. Sponsoring Agency Code

15. Supplementary Notes

16. Abstract

The coolant flow and pressure distributions through a complex air-cooled turbine vane were determined experimentally. Pressure and flow distributions were measured over a range of inlet air flow rates from 0.022 to 0.088 lb/sec (10 to 40 g/sec), inlet pressures from 28 to 73 psia (19 to 50 N/cm^2), and temperatures from 80^o to 1000^o F (300 to 811 K). Computational techniques were developed to predict local values of flow-rate and pressure in future heat transfer tests.

17. Key Words (Suggested by Author(s))		18. Distribution Statement
Turbine cooling	Pin fins	Unclassified - unlimited
Flow distribution	Film cooling	
Pressure distribution	Convection cooling	
Impingement cooling		

19. Security Classif. (of this report)	20. Security Classif. (of this page)	21. No. of Pages	22. Price*
Unclassified	Unclassified	44	$3.00

*For sale by the Clearinghouse for Federal Scientific and Technical Information
Springfield, Virginia 22151

COOLANT PRESSURE AND FLOW DISTRIBUTION THROUGH AN AIR-COOLED VANE FOR A HIGH-TEMPERATURE GAS TURBINE

by John S. Clark, Hadley T. Richards, David J. Poferl, and John N. B. Livingood

Lewis Research Center

SUMMARY

The coolant flow and pressure distributions through the various internal cooling passages of a complex turbine vane were determined experimentally. These distributions were obtained in the leading-edge, midchord, and trailing-edge regions of the vane. Pressure and flow distributions were measured over a range of inlet air flow rates from 0.022 to 0.088 pound per second (10 to 40 g/sec), inlet pressures from 28 to 73 psia (19 to 50 N/cm^2), and temperatures from 80° to 1000° F (300 to 811 K).

Experimental friction pressure drops in the leading edge exit passage and the midchord supply tube were larger than those calculated assuming turbulent flow in smooth tubes but could be correlated with average flow rates. The pressure drop in the trailing-edge suction and pressure side film-cooling slots were correlated with compressible discharge coefficients. The frictional pressure drops in the split trailing edge were correlated with trailing-edge flow rates. Experimental loss coefficients determined from the vane inlet supply tube to the midchord supply tube compared fairly well with predicted values. Pressure distributions were calculated using one-dimensional momentum analyses for those passages of the vanes involving flow ejection or injection through porous walls.

Preliminary three-dimensional heat-transfer computations indicate that vane flow-rate distributions predicted using the experimental correlations will result in a maximum error of $\pm 40^{\circ}$ F (± 22.2 K) in calculated vane metal temperatures.

INTRODUCTION

An experimental investigation was conducted to determine the cooling air flow and pressure distributions inside an air-cooled turbine vane and to compare the experimental

results with theoretical calculations. The internal geometry of the vane selected for this investigation was quite complex and incorporated various cooling concepts in its design. This study is just one portion of a series of experimental coolant flow distribution studies to investigate vane and blade cooling configurations. The results of the initial phase of this series of studies is given in reference 1 which defines the flow through thick-plate orifices with the major component of approach velocity perpendicular to the axis of the orifice.

In order to obtain significant performance gains, the requirement for increased gas turbine-inlet temperatures and the associated turbine vane metal temperatures have pushed heat-resistant materials to the limit of their capabilities, even when the vanes are internally cooled. Therefore, if structural failure of critically stressed turbine components is to be avoided, it is essential that turbine component metal temperatures be accurately predicted.

The ability to accurately calculate flow distributions in complex vanes and blades has not yet been perfected. Sizeable discrepancies exist between calculated and measured vane and blade metal temperatures due, in part, to a lack of knowledge of the flow distribution through the various internal cooling passages.

The Lewis Research Center is currently engaged in a study of advanced turbine vane and blade designs. Reference 2 describes the Lewis test facility that includes a high-temperature engine and a static cascade. The engine and cascade are capable of operating at average inlet gas temperatures up to 2500° F (1645 K) with vanes and blades having a span of about 4 inches (10.2 cm) and a chord of about 2 inches (5.1 cm). Since the vanes supplied with the engine combine convection cooling, film cooling, convective cooling with pin-fins in the split trailing edge, and impingement cooling and since heat-transfer tests of this configuration are to be run initially in the Lewis static cascade and engine, this vane was selected for the flow tests reported herein.

Detailed flow measurements cannot be made during heat-transfer tests on an engine because of space limitations for instrumentation leads. Therefore, it was necessary to instrument a turbine vane and flow test it in a separate flow distribution apparatus in order to experimentally determine the characteristic relations that define cooling-air flow distributions. Tests were run over a range of flow conditions that adequately simulate the expected engine and static cascade test conditions. Air flow rates ranged from 0.022 to 0.088 pound per second (10 to 40 g/sec), pressures ranged from 28 to 73 psia (19 to 50 N/cm^2), and temperatures from about 80° to 1000° F (300 to 811 K). The corresponding engine operating conditions are 0.04 pound per second (18.2 g/sec), 44 psia (30 N/cm^2), and 1200° F (922 K), respectively. These results will be used to analyze the flow distribution in the vane during the static cascade and engine tests.

DESCRIPTION OF APPARATUS

Vane Description

A cross-sectional view of the vane is shown in figure 1. The vane span is about 4 inches (10.2 cm) and the chord is about 2 inches (5.1 cm). Cooling air enters from a supply tube at the top of the vane and flows into a vane tip plenum chamber, at which point the flow divides. Part of the air flows into a leading-edge impingement tube and, by flowing through 16 impingement slots, 0.185 in. (0.47 cm) long and 0.008 to 0.015 in. (0.020 to 0.038 cm) wide, impinges on the internal surface of the vane leading edge. The surface area in this region is increased by chordwise fins. This flow then passes between the fins, around the leading-edge impingement tube in a chordwise direction, into the leading-edge exit passage, and exhausts into the leading-edge collector tube. The remainder of the flow in the tip plenum chamber enters a midchord supply tube and

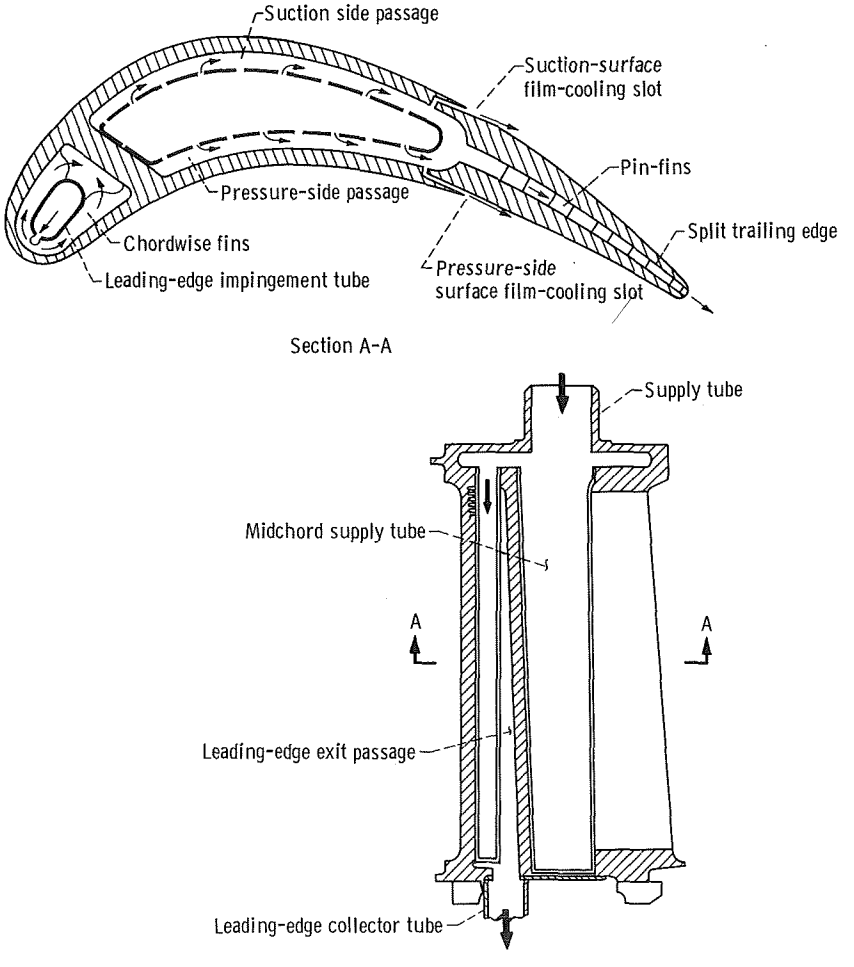

Figure 1. - Vane internal flow configuration.

flows toward the vane hub. This air then impinges on the internal surfaces of the vane suction and pressure sides by flowing through 481 and 334 0.015-inch (0.038-cm) diameter holes on the suction and pressure sides, respectively. This flow then exits through film-cooling slots, on the pressure surface and on the suction surface, and through the split trailing edge, which contains a staggered pin-fin configuration consisting of four rows of oblong pins and one row of round pins. The pressure surface film-cooling slot is a continuous slot 3.65 inches (9.27 cm) by 0.025 inch (0.64 cm), which is fed by 16 metering slots, 0.100 inch (0.25 cm) by 0.021 inch (0.053 cm). The suction surface, contains eight 0.438 inch (1.11 cm) by 0.020 inch (0.51 cm) slots, which are fed by a total of 16 metering slots, 0.075 inch (0.19 cm) by 0.020 inch (0.051 cm). The oblong pins in the trailing edge, 0.15 inch (0.38 cm) by 0.10 inch (0.25 cm) vary in height from 0.070 inch (0.18 cm) to 0.037 inch (0.094 cm), since the split trailing edge is tapered. The round pins have a diameter of 0.080 inch (0.20 cm) and a height of 0.025 inch (0.64 cm).

Flow Apparatus

A flow bench was used to perform the tests described herein. This flow bench was previously used and described in reference 1 and is shown schematically in figure 2. Laboratory service air at 125 psig (86.2 N/cm^2) was dried, filtered, and passed through two successive pressure regulators to a rotameter calibrated for inlet weight-flow measurement. The air was then directed through a triple-pass 25-kilowatt electric heater. The heater could be manually or automatically controlled to provide constant air temperatures up to 1000° F (811 K) for flow rates between 0.01 and 0.1 pound per second (4.54 and 45.4 g/sec). The vane was attached as near to this heater as was practical with well insulated piping.

The air from the vane leading-edge exit passage was ducted to the air cooler and from this point through a throttling valve to a rotameter and then discharged to atmospheric pressure. This permitted controlling back pressure on the leading-edge exit passage. Air that exited through the trailing-edge passages entered a hot air collector and discharged to the atmosphere outside the test cell.

Ambient air tests were also run with the same apparatus with the electric heater bypassed. For these tests, collectors were attached to the vane split trailing edge and the two film-cooling passages and the weight flow from each collector was measured by a rotameter.

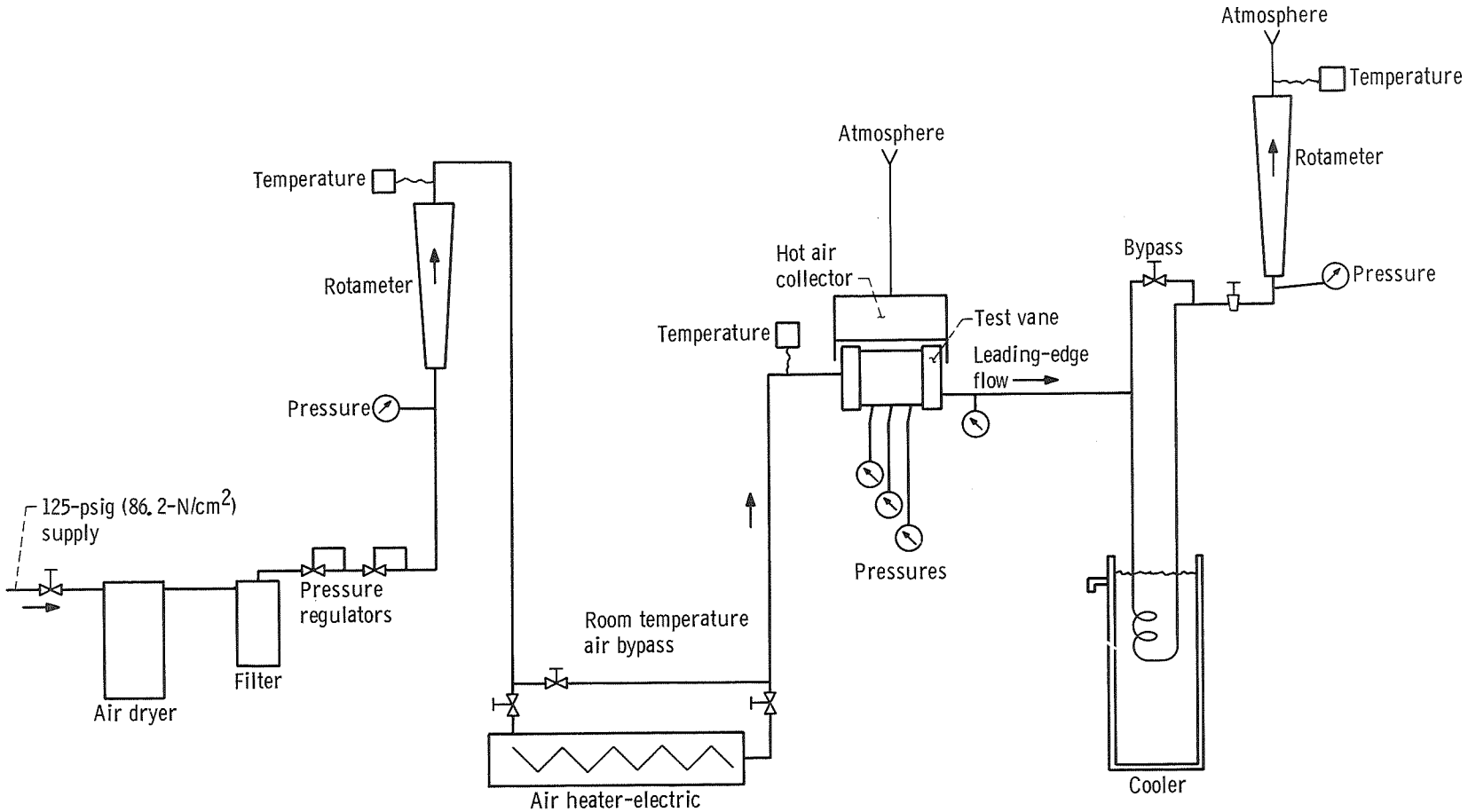

Figure 2. - Flow distribution apparatus for hot tests.

INSTRUMENTATION

Flow Measurements

The flow which entered the vane tip through a supply tube exited through four openings. In order to measure the amount of flow exiting through each of the openings, four flow collectors were fastened to the vane at the following locations: one at the vane base leading-edge region, one covering each of the two film cooling slots, and one surrounding the split trailing edge. Figure 3 shows the trailing edge flow collectors. Symbols are defined in appendix A.

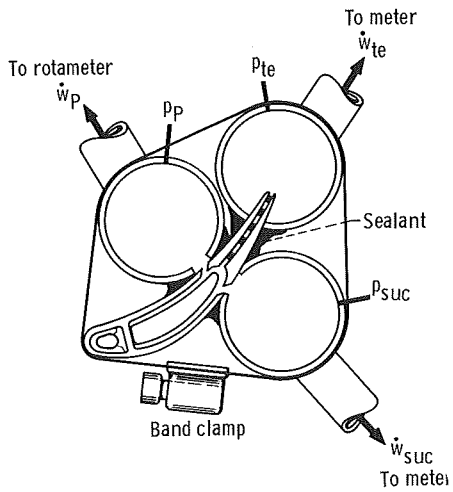

Figure 3. - Trailing-edge collector arrangement.

The leading-edge cooling air collector was a 0.5-inch (1.27-cm) diameter stainless-steel tube which was welded in place to cover the discharge passage in the vane base. The three remaining collectors were closed-end steel cylinders with a contoured slot. For the ambient tests, these cylinders were attached with an air-curing silicone sealant. Band clamps (shown in fig. 3) provided the necessary support for the three collecting tanks to resist the internal pressure. Air from each of these collectors exited through 0.5-inch (1.27-cm) diameter tubing.

The system described in the preceding paragraph was satisfactory for testing at ambient temperature. However, even with the addition of a high-temperature sealant, which was continuous-use rated at 600° F (589 K), the three collectors could not be sealed with the vane assembly raised to 200° F (366 K) or higher. For tests at temperatures above ambient, therefore, only the leading-edge collector could be used.

Rotameters were installed in the inlet supply piping and downstream of each of the collectors. The rotameters used were commercial models, calibrated for air at densities corresponding to those expected during operation. The accuracy to be expected from these meters was 1/2 percent of full scale. For elevated air temperature tests, the heated air was cooled to room temperature before being passed through the rotameter as shown in figure 2.

Pressure Measurements

The vane was equipped with 23 static pressure taps. The locations of these taps are shown on figure 4. For the leading-edge region, three pressure taps were provided: at the entrance to the leading-edge impingement tube (location 1), at the entrance to the leading-edge exit passage (location 2), and in the leading-edge collector (location 3). For the midchord region, three spanwise pressure taps were located in the midchord supply tube (locations 4 to 6). Also, six pressure taps were located in each of the suction side and pressure side flow channels (locations 7 to 10, 7' to 10', and 7'' to 10'') as shown in figure 4. Pressure taps 9, 9', and 9'', and 10, 10', and 10'' are located within 0.15 inch (0.38 cm) of the entrance to the metering slots that feed the suction and pressure surface film cooling slots. Pressure taps 7, 7', and 7'' and 8, 8', and 8'' are located within 0.10 inch (0.25 cm) of the leading-edge end of the suc-

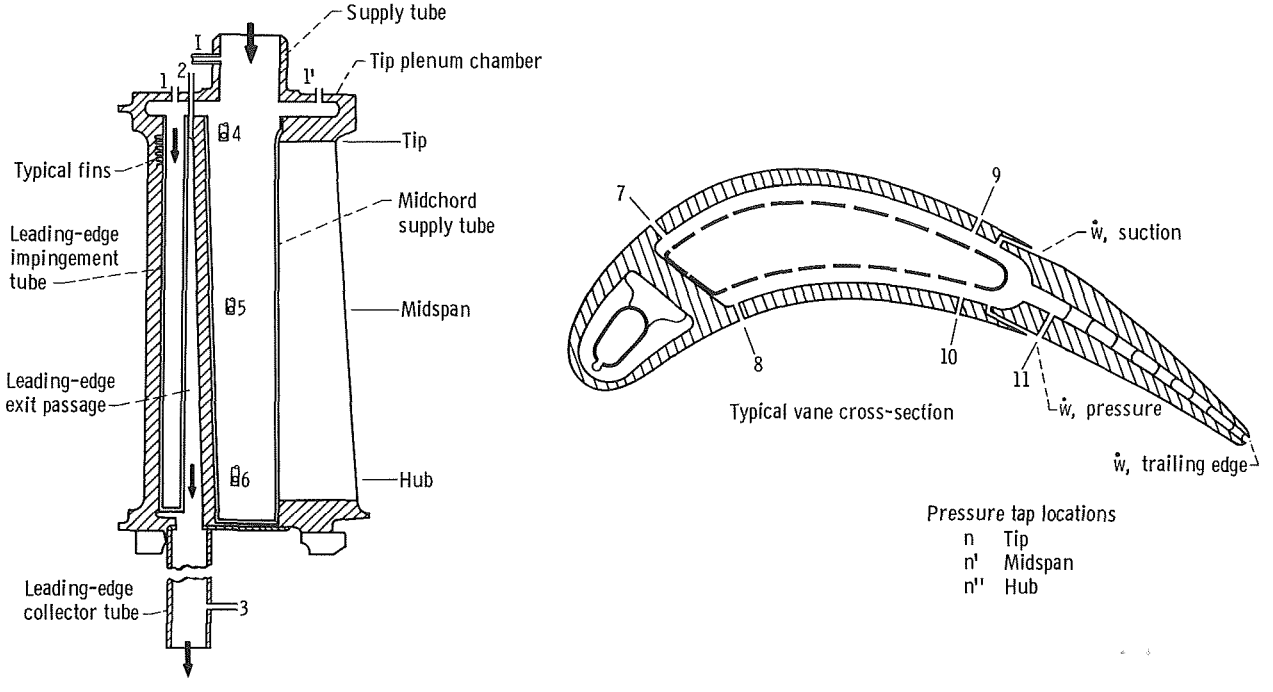

Figure 4. - Slave vane pressure instrumentation.

tion and pressure side passages. The location of these pressure taps in the midchord region is critical: if a static pressure tap is located directly opposite an impingement hole in the midchord supply tube, the pressure reading will be affected by the impinging flow. Three spanwise trailing-edge pressure taps were located within 0.10 inch (0.25 cm) of the entrance to the split trailing edge (locations 11, 11', and 11''). Pressure taps were also included in each of the collectors as shown on figure 3, in the tip plenum chamber (locations 1 and 1'), and in the inlet supply tube (location I) as shown on figure 4.

The pressure taps were connected to pressure gages through a selector switch. Delays in balancing pressure readings after changing the selector switch position were no more than 5 seconds. All pressures measured were estimated to be accurate to within ±0.05 psi (0.034 N/cm^2).

Air Temperature Measurements

Inlet air temperature was measured at the same location as the inlet pressure (location I) by a thermocouple probe inserted into the airstream. The temperature measured by the probe was read on a null balance potentiometer to the nearest 5° F (2.8 K).

TEST PROCEDURE

Ambient Tests with Trailing-Edge Collectors

The primary test objective was to determine the flow and pressure distribution characteristics for the conditions expected during engine operation. Since the vane was equipped with collectors at each of the cooling-air exits for 35 ambient air tests, it was possible to adjust the exit back-pressure in each collector to equal the expected vane midspan pressures (when subjected to cascade or engine gas flow). Sixteen tests were run with back-pressures set to the pressures expected in the engine. Thus, the expected pressure and flow rate could be simulated. Tests were also run with various other back-pressure conditions to determine what effect back-pressure had on the flow and pressure distribution. For example, five tests were run with equal back-pressures in the collectors at the two film cooling slots and the split trailing edge. Seven runs were made with the trailing-edge passage closed and equal pressures set in the film cooling slot collectors. Five runs were made with the pressure surface film-cooling slot closed, and two runs were made with both the pressure and suction surface film-cooling slots closed.

Tests Without Trailing-Edge Collectors

For tests at air temperatures higher than ambient (and more nearly equal to the expected 1200° F (922 K) cooling air in the engine), only the collector at the leading-edge exit passage could be sealed; therefore, cooling air flowing through the other exits was exhausted to ambient pressure. Only the inlet pressure and the leading-edge exit backpressure could be varied for these tests. Tests were run for leading-edge exit pressures of 38 and 25 psia (26 and 17 N/cm^2). For all tests, the total cooling air flow rate into the vane was varied over a range of values sufficient to cover the expected rates in engine test runs.

Eighty-one runs were made without trailing-edge collectors. Forty runs were made for ambient temperature cooling air, nine for 200° F (366 K) cooling air, 15 for 600° F (589 K) cooling air, one for 850° F (728 K) cooling air, six for 950° F (783 K) cooling air, and 10 for 1000° F (811 K) cooling air. Thirteen runs were made with the leading-edge exit collector pressure set at 25 psia (17 N/cm^2); 68 runs had the leading-edge collector pressure set at 38 psia (26 N/cm^2).

ANALYSIS OF DATA

The prediction of flow distribution in a geometrically complicated structure, such as an air-cooled turbine vane, may be accomplished by dividing the cooling passages into a network that includes all possible flow paths. Then, starting from known boundary conditions, each passage within the network may be analyzed using known one-dimensional flow equations. In the case of parallel passages, initial estimates of flow distribution have to be revised until the pressure drop is the same for each passage. For passages in series, the pressure drop is simply the sum of the individual pressure drops of each of the components. However, effective air-cooled vanes will often consist of a combination of parallel and series passages with some passages not amenable to a one-dimensional flow analysis.

Pressure-Drop Equations

The pressure drop across a single passage may be found by calculating (1) entrance loss, (2) exit loss, (3) friction loss, and (4) momentum losses within the passage. There are many portions of the vane where these losses occur. Determination of these losses will be made with the use of the following equations.

Entrance loss. - The entrance loss due to a sudden contraction in an incompressible flow may be calculated from

$$\Delta P = K_L \frac{G^2}{2\rho} \tag{1}$$

The coefficient K_L has been found empirically to be approximately 0.5 for a square or sharp inlet in turbulent flow, and approximately 0.04 for a well-rounded or bellmouth inlet (ref. 3). Obviously, these coefficients are a strong function of the geometry of the particular inlet.

Exit loss. - The total pressure drop resulting from a sudden enlargement may be calculated from

$$\Delta P = \frac{(1 - \epsilon)^2 G^2}{2\rho} \tag{2}$$

where ϵ is the ratio of the upstream flow area to the downstream flow area.

Friction loss and momentum change. - The following equation describes steady one-dimensional fluid flow.

$$dp + 4f \frac{\rho V^2}{2} \frac{dx}{D_h} + \rho V \, dV = 0 \tag{3}$$

For a constant area passage with no heat addition or pumping, the continuity equation requires that the velocity remain unchanged for an incompressible ideal fluid. Therefore, the pressure change is seen to be caused by fluid friction only. This friction pressure drop is

$$(\Delta p)_{fr} \equiv 4f \frac{L\rho V^2}{2D_h} \tag{4}$$

where f is the Fanning friction factor. This is really the definition of the friction factor.

In general, the area of the passage is not constant, however, and equation (3) must be integrated, including the effects of the change of velocity. Thus,

$$\int_2^1 dp = \int_1^2 \frac{\rho V^2}{2} \frac{4f}{D_h} dx + \int_1^2 \rho V \, dV \tag{5}$$

or

$$p_1 - p_2 = (\text{Friction pressure drop}) + (\text{Momentum pressure drop}) \tag{6}$$

The tests reported herein were isothermal. When nonisothermal tests are run, the effect of coolant temperature rise must be accounted for in equation (6).

Relation Between Flow Rate and $\rho \Delta p_{fr}$

If, in equation (4), ρV is replaced by $\dot{w}/A$ and correlations of the friction factor f for laminar and turbulent flow are inserted, relations between $\rho \Delta p_{fr}$ and $\dot{w}$ can be obtained:

for laminar flow,

$$f = \frac{16}{Re} \tag{7}$$

for turbulent flow,

$$f = \frac{0.046}{Re^{0.2}} \tag{8}$$

for smooth tubes with $5000 \leq Re \leq 200\,000$ (ref. 4). In either case,

$$Re = \frac{\dot{w}}{A} \frac{D_h}{\mu} \tag{9}$$

Substitution of equations (7) or (8) and (9) into equation (4) yields

$$\rho \Delta p_{fr} = \left(\frac{32 L \mu}{A D_h^2} \right) \dot{w} \tag{10}$$

for laminar flow and

$$\rho \Delta p_{fr} = \left(\frac{0.092 \, L \mu^{0.2}}{A^{1.8} D_h^{1.2}} \right) \dot{w}^{1.8} \tag{11}$$

for turbulent flow.

Pin-Fin Friction Factor

Equations (10) and (11) were applied to the leading-edge region. For the trailing edge, a new friction factor equation was required because of the presence of pin fins in the passages. For this case, (ref. 5)

$$f = \rho \Delta p_{fr} \frac{1}{2n} \frac{1}{\left(\frac{\dot{w}}{A_{min}} \right)^2} \tag{12}$$

Here n is the number of pin fins in the flow direction (equal to 5 in this case) and A_{min} is the minimum flow area between pins in the trailing-edge passage.

Jacob (ref. 6) developed a correlation of friction factor for pin-finned passages. This correlation is

$$f = Re_d^{-0.16} \left[0.25 + \frac{0.1175}{(a - 1)^{1.08}} \right] \tag{13}$$

where

$$a = \frac{S_t}{d}$$

This correlation was used to compare with the experimental data obtained in the split trailing edge. These results will be discussed in the RESULTS AND DISCUSSION section of this report.

One-Dimensional Momentum-Flow Analysis

An analytical method for calculating flow in a rotating passage with injection through a porous wall is presented in reference 7. Equation (5) of reference 7 is

$$\left[1 - \left(\frac{\dot{w}}{A}\right)^2 \frac{RT}{p_{in}^2}\right] \frac{dp_{in}}{dx} = \frac{p_{in} r\omega^2}{RT} \cos\beta - \frac{2RT}{p_{in}} \frac{\dot{w}}{A} \frac{d\frac{\dot{w}}{A}}{dx} - \left(\frac{\dot{w}}{A}\right)^2 \frac{R}{p_{in}} \left(\frac{4fT}{2D_h} + \frac{dT}{dx} + \frac{T}{A}\frac{dA}{dx}\right) \tag{14a}$$

For application herein (a stationary vane) the first term in the right side of the equation is deleted since it is the rotational term. An assumption made in the present application was that there was no temperature rise in the coolant. Equation (14a) then becomes

$$\left[1 - \left(\frac{\dot{w}}{A}\right)^2 \frac{RT}{p_{in}^2}\right] \frac{dp_{in}}{dx} = - \frac{2RT}{p_{in}} \frac{\dot{w}}{A} \frac{d\frac{\dot{w}}{A}}{dx} - \left(\frac{\dot{w}}{A}\right)^2 \frac{R}{P_{in}} \left(\frac{4fT}{2D_h} + \frac{T}{A}\frac{dA}{dx}\right) \tag{14b}$$

This simplified equation was used to predict pressure variations in the vane leading-edge exit passage and midchord suction and pressure side passages. Each of these passages had increasing cooling flow in the flow direction.

The equation used for predicting pressures in passages with flow ejection, that is, decreasing flow in the flow direction is

$$\left[1 - \left(\frac{\dot{w}}{A}\right)^2 \frac{RT}{p_{in}^2}\right] \frac{dp_{in}}{dx} = - \frac{RT}{p_{in}} \frac{\dot{w}}{A} \frac{d\frac{\dot{w}}{A}}{dx} - \left(\frac{\dot{w}}{A}\right)^2 \frac{R}{p_{in}} \left(\frac{4fT}{2D_h} + \frac{dT}{dx}\right) \tag{14c}$$

The derivation of this equation is given in appendix B.

For the purpose of this analysis, it was assumed that there was no temperature gradient in any cooling passage. The resulting equation (eq. (14d)) was used to calculate the theoretical pressure distributions in the leading-edge impingement tube and the midchord supply tube. However, when heat-transfer tests are run in the cascade and engine, the dT/dx term in equation (14a) and (14c) must be retained.

$$\left[1 - \left(\frac{\dot{w}}{A}\right)^2 \frac{RT}{p_{in}^2}\right] \frac{dp_{in}}{dx} = - \frac{RT}{p_{in}} \frac{\dot{w}}{A} \frac{d\frac{\dot{w}}{A}}{dx} - \left(\frac{\dot{w}}{A}\right)^2 \frac{R}{p_{in}} \frac{4fT}{2D_h} \tag{14d}$$

Equations (14b) and (14d) were both solved numerically using a fourth-order Runge-Kutta technique.

The differences between the right-hand terms of equations (14b) and (14d) are due to the use of different flow models for the cases of flow injection and ejection. The flow model assumed in reference 7 is considered applicable only to the case of injected flow. The flow model for the flow ejection case is shown in figure 5 where the ejected flow

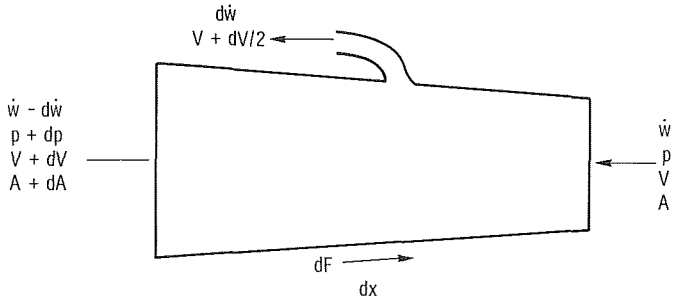

Figure 5. - Flow channel control surface with flow ejection.

leaves the control volume with a velocity vector the same as that of the main stream. In contrast, in the flow injection case, the flow is assumed to enter the control volume with no momentum in the direction of flow.

Midchord Chordwise Flow Rate Calculation

The air discharging from the midchord supply tube holes flows in a chordwise direction to the rear of the vane where it splits and discharges through the film-cooling slots and the split trailing edge. The flow rate along each side of the insert in the chordwise direction is required to determine the total pressure upstream of the film-cooling slots. This flow rate will also be required in the heat-transfer tests to determine heat-transfer coefficients in this region.

The average pressure inside the midchord supply tube is calculated using Simpson's rule:

$$\bar{p}_{mc,\,i} = \frac{1}{6}\left(p_4 + 4p_5 + p_6\right) \tag{15}$$

Also, the chordwise passage average inlet and outlet pressures are found from

$$\left.\begin{aligned}
\bar{p}_7 &= \frac{1}{6}\left(p_7 + 4p_{7'} + p_{7''}\right) \\
\bar{p}_9 &= \frac{1}{6}\left(p_9 + 4p_{9'} + p_{9''}\right) \\
\bar{p}_8 &= \frac{1}{6}\left(p_8 + 4p_{8'} + p_{8''}\right) \\
\bar{p}_{10} &= \frac{1}{6}\left(p_{10} + 4p_{10'} + p_{10''}\right)
\end{aligned}\right\} \tag{16}$$

The ideal flow rate through an impingement hole is then found from

$$\left.\begin{aligned}
\dot{w}_{suc,\,in,\,id} &= \sqrt{\frac{2A^2}{R}\left(\frac{\gamma}{\gamma-1}\right)\frac{(\bar{p}_7)^2}{T}\left[1-\left(\frac{\bar{p}_7}{\bar{P}_{mc,\,i}}\right)^{(\gamma-1)/\gamma}\right]\left(\frac{\bar{P}_{mc,\,i}}{\bar{p}_7}\right)^{2(\gamma-1)/\gamma}} \\
\dot{w}_{suc,\,out,\,id} &= \sqrt{\frac{2A^2}{R}\left(\frac{\gamma}{\gamma-1}\right)\frac{(\bar{p}_9)^2}{T}\left[1-\left(\frac{\bar{p}_9}{\bar{P}_{mc,\,i}}\right)^{(\gamma-1)/\gamma}\right]\left(\frac{\bar{P}_{mc,\,i}}{\bar{p}_9}\right)^{2(\gamma-1)/\gamma}} \\
\dot{w}_{p,\,in,\,id} &= \sqrt{\frac{2A^2}{R}\left(\frac{\gamma}{\gamma-1}\right)\frac{(\bar{p}_8)^2}{T}\left[1-\left(\frac{\bar{p}_8}{\bar{P}_{mc,\,i}}\right)^{(\gamma-1)/\gamma}\right]\left(\frac{\bar{P}_{mc,\,i}}{\bar{p}_8}\right)^{2(\gamma-1)/\gamma}} \\
\dot{w}_{p,\,out,\,id} &= \sqrt{\frac{2A^2}{R}\left(\frac{\gamma}{\gamma-1}\right)\frac{(\bar{p}_{10})^2}{T}\left[1-\left(\frac{\bar{p}_{10}}{\bar{P}_{mc,\,i}}\right)^{(\gamma-1)/\gamma}\right]\left(\frac{\bar{P}_{mc,\,i}}{\bar{p}_{10}}\right)^{2(\gamma-1)/\gamma}}
\end{aligned}\right\} \tag{17}$$

in these equations A is the area of one hole.

This analysis assumes that the Mach number is low in the midchord supply tube; therefore, the average total pressure within the tube may be approximated by the average static pressure $\bar{p}_{mc,i}$. Thus, the average ideal flow rate per hole on each side is

$$\left.\begin{aligned} \dot{w}_{suc,id} &= \frac{1}{2}\left(\dot{w}_{suc,in,id} + \dot{w}_{suc,out,id}\right) \\ \dot{w}_{p,id} &= \frac{1}{2}\left(\dot{w}_{p,in,id} + \dot{w}_{p,out,id}\right) \end{aligned}\right\} \tag{18}$$

and the total ideal flow rate per side is found by multiplying the ideal flow rate per hole by the number of holes on each side (481 holes on the suction side, 334 holes on the pressure side).

Then, the normalized flow rate may be calculated for each side:

$$\left.\begin{aligned} \dot{w}_{suc,N} &= 481\dot{w}_{suc,id} \times \frac{\dot{w}_{mc,meas}}{(481\dot{w}_{suc,id}) + (334\dot{w}_{p,id})} \\ \dot{w}_{p,N} &= 334\dot{w}_{p,id} \times \frac{\dot{w}_{mc,meas}}{(481\dot{w}_{suc,id}) + (334\dot{w}_{p,id})} \end{aligned}\right\} \tag{19}$$

Film-Cooling Slots Discharge Coefficients

Turning losses and expansion losses occur when cooling air passes through the suction and pressure surface film-cooling slots due to changes in the coolant flow direction and abrupt flow area changes in the slot passages. As a consequence these slots may not behave as ideal nozzles. Therefore, an attempt was made to correlate experimental discharge coefficients with coolant flow rate through the slots rather than with Reynolds number, the usual parameter.

The ideal flow rate through a convergent nozzle is found from

$$\dot{w}_{id} = \rho_{out} A \sqrt{\frac{2\gamma RT_{in}}{\gamma - 1}\left[1 - \left(\frac{p_{out}}{p_{in}}\right)^{(\gamma-1)/\gamma}\right]} \tag{20}$$

In this expression, the outlet conditions correspond to the jet outlet static conditions, while the inlet conditions are total quantities. The areas used are the minimum flow cross-sectional areas in the slots; that is, 0.0293 square inch (0.189 cm^2) for the pressure side and 0.0222 sqaure inch (0.145 cm^2) for the suction side. The discharge coefficient is

$$C_D = \frac{\dot{w}_{meas}}{\dot{w}_{id}} \tag{21}$$

These expressions are used to calculate discharge coefficients for the film-cooling slots on the pressure and suction surfaces. The jet static pressure is assumed to be the static pressure measured in the collector passages. The inlet total conditions are calculated from the measured static conditions upstream of the slot and the calculated suction side and pressure side flow rates. The total pressures at the entrances to the film-cooling slots are calculated with equation (22).

$$\left.\begin{aligned} P_{in,\,suc} &= \bar{p}_9 \left[1 + \left(\frac{\gamma - 1}{2}\right) M_{suc}^2\right]^{\gamma/(\gamma-1)} \\ P_{in,\,p} &= \bar{p}_{10} \left[1 + \left(\frac{\gamma - 1}{2}\right) M_p^2\right]^{\gamma/(\gamma-1)} \end{aligned}\right\} \tag{22}$$

The area A_{in} refers to the cross-sectional flow area of 0.118 square inch (0.761 cm^2) in either the suction side or the pressure side passage and the Mach numbers are obtained from equation (23).

$$\left.\begin{aligned} M_{suc} &= \frac{\dot{w}_{suc,\,N}}{\rho_{in} A_{in} a_v} \\ M_p &= \frac{\dot{w}_{p,\,N}}{\rho_{in} A_{in} a_v} \end{aligned}\right\} \tag{23}$$

RESULTS AND DISCUSSION

Leading-Edge Region

Loss coefficient of flow entering leading edge impingement tube. - An attempt was made to determine the loss coefficient from the inlet supply tube to the entrance of the leading-edge impingement tube basing the pressure at the entrance to the leading-edge impingement tube on p_1. However, leading-edge data indicate that the total pressure in the leading-edge impingement tube is higher than the total pressure in the inlet supply tube. Since this is impossible, it must be concluded that the static pressure measured at location 1 is not equal to the static pressure inside the leading-edge impingement tube. Therefore, it was not possible to determine the loss coefficient from location I to location 1.

Pressure drop through leading-edge exit passage. - The leading-edge exit passage was a noncircular passage that increased in size from the vane tip to the hub. Air from the chordwise fins entered the passage along the entire length of the passage and finally discharged into the leading-edge collector tube. The measured static pressure at the passage tip is p_2 and p_3 is the measured static pressure in the leading-edge collector tube. The Mach number was calculated in the leading-edge collector tube, and in the area at the leading-edge exit, just above the collector tube (see fig. 6). The maxi-

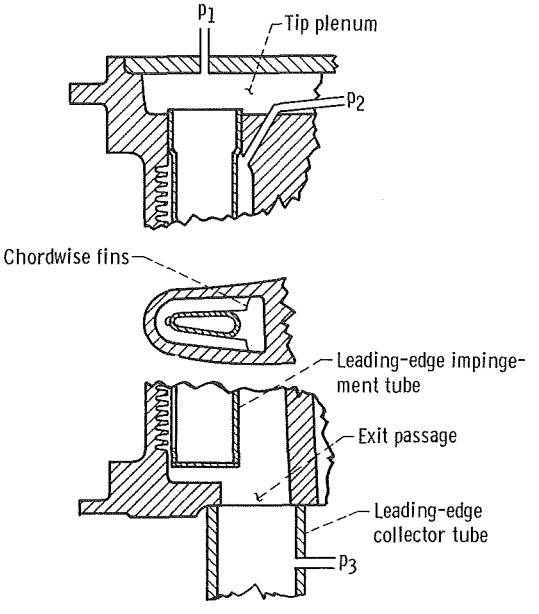

Figure 6. - Leading-edge cooling scheme.

mum Mach number for any of the runs was 0.116 for the collector tube and 0.35 for the exit passage. For most of the runs, however, the Mach numbers were much lower than these values. Thus, it was expected that the incompressible equations should yield reasonable results for this region.

The exit loss from the passage into the leading-edge collector was found using equation (2) iteratively. The loss was a function of the density in the upstream passage, which was a function of the unknown upstream pressure. The momentum pressure change from location 2 to the leading-edge exit was calculated by use of equation (5) and subtracted from the total pressure drop to yield the friction pressure drop $(\Delta p_{fr})_{2\text{-le, x}}$.

Figure 7 shows a plot of the measured $(\rho\ \Delta p_{fr})_{2\text{-le, x}}$ as a function of average leading-edge flow rate; predicted turbulent values calculated using equation (11) are also shown on the figure. Since equation (11) was derived based on a constant velocity in a constant area duct, average values of flow rate, density, and duct area were used to calculate predicted values of the pressure-drop parameter. The density was calculated from the average of the measured pressure at location 2 and the calculated leading-edge exit pressure. The area and hydraulic diameter were evaluated at the span position

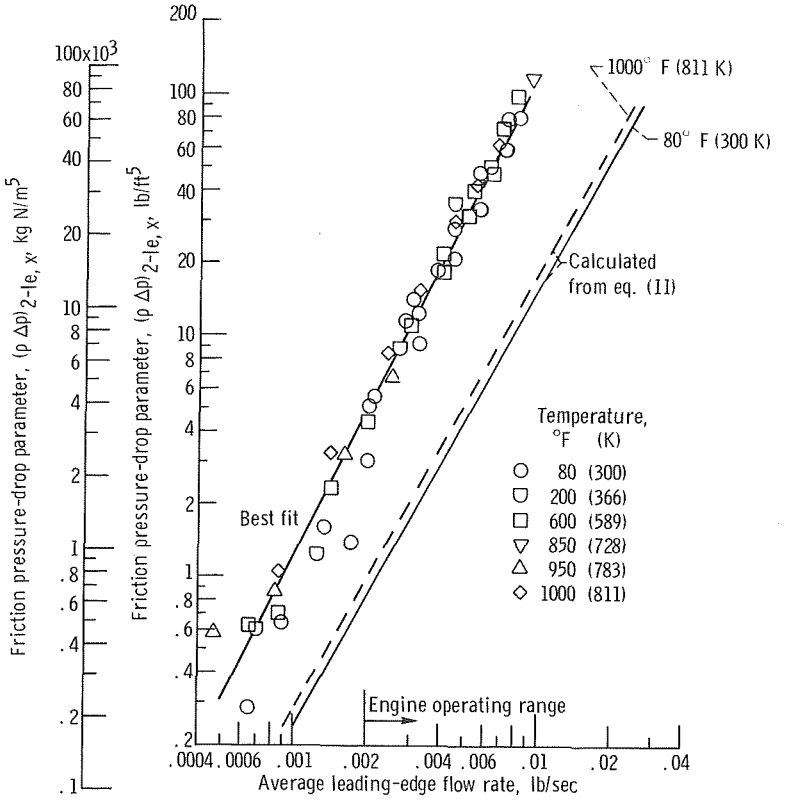

Figure 7. - Friction pressure-drop parameter for leading-edge exit passage as function of average leading-edge flow rate.

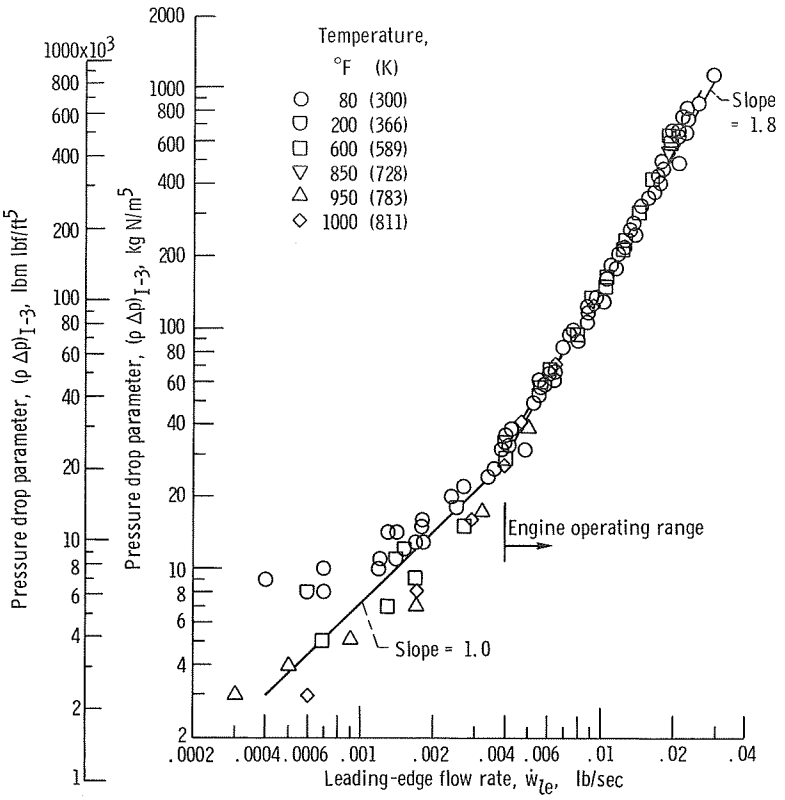

Figure 8. - Friction pressure-drop parameter for leading-edge as function of leading-edge flow rate.

where the flow in the leading-edge exit passage was calculated to be one-half of the total leading-edge flow. The slope of the data in figure 7 indicates that the flow through this passage is turbulent and that the experimental pressure drop parameter can be empirically correlated with leading-edge exit passage flow rate. However, the turbulent smooth tube friction factor equation predicts experimental friction pressure drops considerably less than the experimental values. This can be expected, however, since equation (11), which was used in an attempt to obtain the usual correlation, is based on constant passage area, density, and velocity, whereas these quantities actually vary along the length of the leading-edge exit passage. Furthermore, the momentum drop associated with the addition of mass along the passage length is not accounted for in equation (5). A method for calculating the pressure distribution in the leading-edge exit passage which accounts for flow addition along the length of the passage will be presented in a later section of this report.

Overall leading edge. - An attempt was made to correlate the overall pressure drop from the inlet supply tube (location I), to the leading-edge collector tube (location 3). Figure 8 shows $(\rho\ \Delta p)_{I-3}$ as a function of leading-edge flow rate. The density was cal-

culated from the average of p_I and p_3, and the pressure drop is the measured overall pressure drop from I to 3. It includes:

(1) Entrance loss into the leading-edge impingement tube

(2) Exit and vortex losses from the leading-edge impingement tube

(3) Friction pressure drop within the leading-edge impingement tube, chordwise fins, and exit passage

(4) Turning loss and/or exit loss from the chordwise fins into the exit passage

(5) Momentum pressure drop

(6) Exit pressure drop from the leading-edge exit passage into the collector tube

Since these tests were isothermal, the momentum change due to the differences in density and velocity in the supply tube and leading-edge collector tube were negligible. During subsequent engine and cascade heat-transfer tests, this momentum pressure drop must be accounted for before using figure 8. The data shown in figure 8 indicate some of the same characteristics as the data shown in figure 7. At the higher flow rates the flow behaves with a turbulent nature (slope ~1.8), but at the lower flows, laminar characteristics are noted (slope approaching 1.0). This curve will be used to predict leading-edge flow rate in the future static cascade and engine tests. The pressures at I and 3 will be measured in these tests. From these measurements the ordinate of figure 8 is completely defined, and the flow rate can be predicted after accounting for the momentum pressure drop. The data shown on figure 8 for flow rates less than about 0.004 pound per second (1.81 g/sec) are below the range that will be run in either the static cascade or the engine, and thus the data scatter in this area is not as bothersome as it might first appear. Uncertainty in the experimental pressure and flow measurements contributed significantly to the data scatter in this area.

Theoretical calculation of static-pressure change through the leading-edge region. - An attempt was made to theoretically predict the static-pressure profile in the leading-edge impingement tube and exit passage. Equation (14b) was used to calculate the static-pressure profile in the leading-edge exit passage, and equation (14d) was used to calculate the static-pressure profile in the impingement tube.

The following assumptions were made in determining the static-pressure profiles in the leading-edge impingement tube and in the leading-edge exit passage:

(1) The temperature of the air remains constant, $dT/dx = 0$.

(2) There is no rotation, $\omega = 0$.

(3) The flow per unit area in the leading-edge exit passage varied linearly from the passage inlet to the passage exit.

(4) The flow remaining in the leading-edge impingement tube at a given distance from the passage inlet is equal to the total leading-edge flow rate minus the flow in the leading-edge exit passage at that point.

TABLE I. - COMPARISON OF EXPERIMENTAL AND THEORETICAL

STATIC-PRESSURE RATIOS IN VANE PASSAGES

Vane region	Cooling air flow rate				Cooling-air temperature		Static-pressure ratio	
	Leading edge		Midchord				Theoretical	Experimental
	lb/sec	g/sec	lb/sec	g/sec	^{o}F	K		
Leading edge impingement tube, p_e/p_1	0.0163	7.40	0.0671	30.5	80	300	1.07	(a)
Leading edge exit passage, p_e/p_2	↓	↓	↓	↓	↓	↓	.88	0.90
Midchord supply tube, p_6/p_4	↓	↓	↓	↓	↓	↓	1.09	1.05
Midchord supply tube, p_5/p_4	↓	↓	↓	↓	↓	↓	1.07	1.05
Midchord passage, suction side, p_9/p_7	↓	↓	↓	↓	↓	↓	.95	.99
Midchord passage, pressure side, p_{10}/p_8	↓	↓	↓	↓	↓	↓	.98	.95
Leading edge impingement tube, p_e/p_1	.0005	.22	.0317	14.4	1000	811	1.00	(a)
Leading edge exit passage, p_e/p_2	↓	↓	↓	↓	↓	↓	1.00	1.00
Midchord supply tube, p_6/p_4	↓	↓	↓	↓	↓	↓	1.09	1.09
Midchord supply tube, p_5/p_4	↓	↓	↓	↓	↓	↓	1.08	1.08
Midchord passage, suction side, p_9/p_7	↓	↓	↓	↓	↓	↓	.95	.99
Midchord passage, pressure side, p_{10}/p_8	↓	↓	↓	↓	↓	↓	.97	.96
Leading edge impingement tube, p_e/p_1	.0064	2.91	.0368	16.7	1000	811	1.04	(a)
Leading edge exit passage, p_e/p_2	↓	↓	↓	↓	↓	↓	.95	.95
Midchord supply tube, p_6/p_4	↓	↓	↓	↓	↓	↓	1.10	1.09
Midchord supply tube, p_5/p_4	↓	↓	↓	↓	↓	↓	1.08	1.09
Midchord passage, suction side, p_9/p_7	↓	↓	↓	↓	↓	↓	.95	.99
Midchord passage, pressure side, p_{10}/p_8	↓	↓	↓	↓	↓	↓	.97	.96
Leading edge impingement tube, p_e/p_1	.0109	4.95	.0441	20.0	1000	811	1.08	(a)
Leading edge exit passage, p_e/p_2	↓	↓	↓	↓	↓	↓	.85	.86
Midchord supply tube, p_6/p_4	↓	↓	↓	↓	↓	↓	1.10	1.10
Midchord supply tube, p_5/p_4	↓	↓	↓	↓	↓	↓	1.08	1.10
Midchord passage, suction side, p_9/p_7	↓	↓	↓	↓	↓	↓	.95	.99
Midchord passage, pressure side, p_{10}/p_8	↓	↓	↓	↓	↓	↓	.97	.96

[a]Insufficient experimental data.

(5) The friction factor was chosen for flow in smooth pipes (e.g., eq. (8)) where the Reynolds number is determined with the passage hydraulic diameter at midspan.

(6) The flow area of the leading-edge impingement tube is constant.

(7) The flow area of the leading-edge exit passage varies linearly with distance from the passage entrance.

(8) The static pressure at the entrance to the leading-edge impingement tube is assumed equal to the static pressure measured in the plenum directly above the impingement tube entrance.

Tneoretical predictions of static pressure change in the leading-edge passage of the vane were made for the following four cases:

(1) High flow rate at ambient temperature

(2) Low flow rate at elevated temperature

(3) Medium flow rate at elevated temperature

(4) High flow rate at elevated temperature

These cases were chosen in order to evaluate the adequacy of the theory to predict pressure changes over a representative range of flows and temperatures.

The results of the calculations for the leading-edge region are given in table I for each of the cases listed. The theoretical and experimental leading-edge data for the case of high flow at elevated temperature are also shown in figure 9. Data for the midchord region are also presented in figure 9 and will be discussed later. The ratio of static pressure along the passages to the inlet static pressure is plotted as a function of dimensionless distance from the passage entrance. It is interesting to note that a pressure rise from tip to hub is predicted for the leading-edge impingement tube; whereas

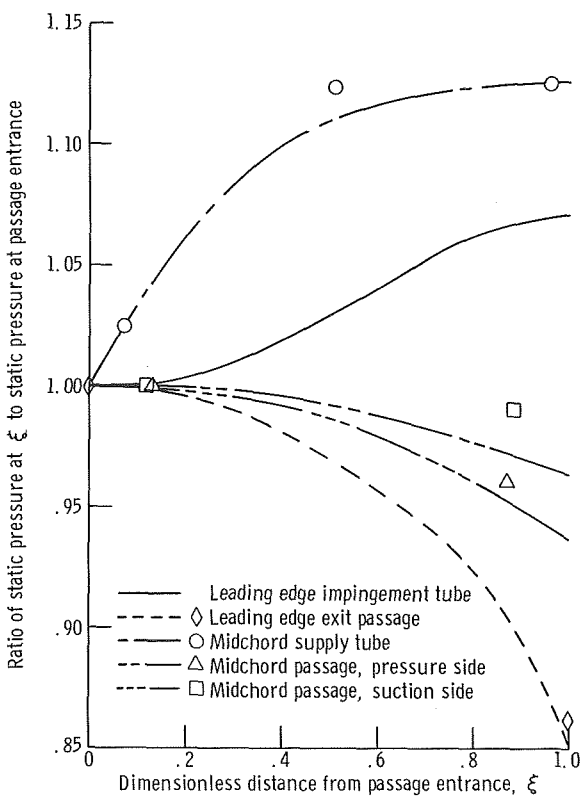

Figure 9. - Static-pressure profiles in slave vane passages for case of high vane cooling flow at elevated temperature. Leading edge flow, 0.0109 pound per second (4.95 g/sec); midchord flow, 0.0441 pound per second (20.0 g/sec), cooling-air temperature, 811 K.

a pressure drop from tip to hub is predicted for the exit passage. This is the result of flow being ejected from the leading-edge impingement tube and injected into the exit passage. Since only the pressure near the entrance to the leading-edge impingement tube was measured, it was not possible to compare the theoretical static-pressure rise prediction with experimental data. However, experimental data were available for the leading-edge exit passage, and the theoretical static-pressure ratios obtained agree with the experimental results.

The calculated pressure differences between the leading-edge impingement tube and the leading-edge exit passage are shown in figure 10. The dimensionless pressure ratio, defined as the difference in static pressure between the leading-edge impingement tube and exit passage divided by the static pressure difference at the passage entrance is plotted as a function of dimensionless distance from the passage entrance. Since the static pressure in the leading-edge impingement tube increases with distance from the passage entrance, whereas the reverse is true for the leading-edge exit passage, the pressure difference between them will increase with increasing distance from the passage entrance as shown in figure 10. Inasmuch as the pressure at the inlet of the

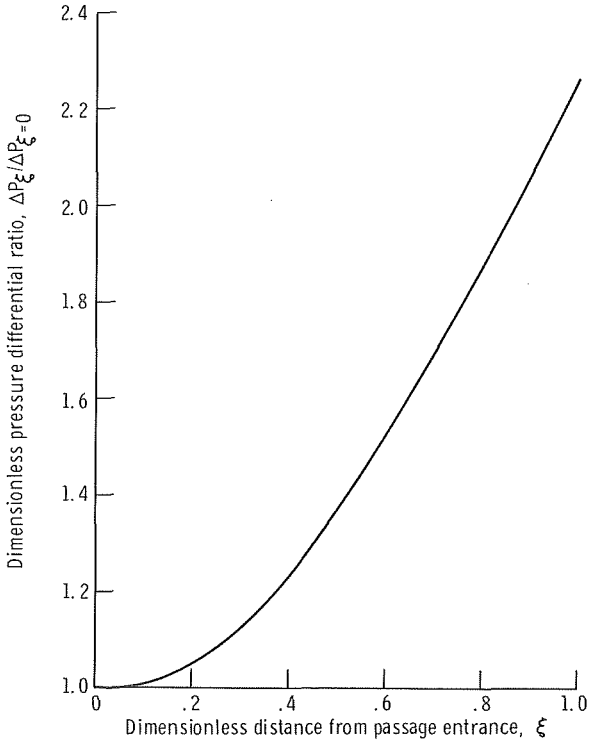

Figure 10. - Pressure differential between leading-edge impingement tube and leading-edge exit passage for the case of high cooling flow at elevated temperature. Leading edge flow, 0.0109 pound per second (4.959/sec); midchord flow, 0.0441 pound per second (20.09/sec); cooling-air temperature, 1000° F (811).

leading-edge impingement tube may not be exactly equal to the measured pressure in the plenum above it, the results for the leading-edge impingement tube pressure distributions and, therefore, the pressure differences between the leading-edge impingement tube and the leading-edge exit passage may be somewhat inaccurate. However, the general trends indicated should be correct.

Midchord Region

Entrance loss. - Since the measured pressure in the inlet supply tube p_I and the

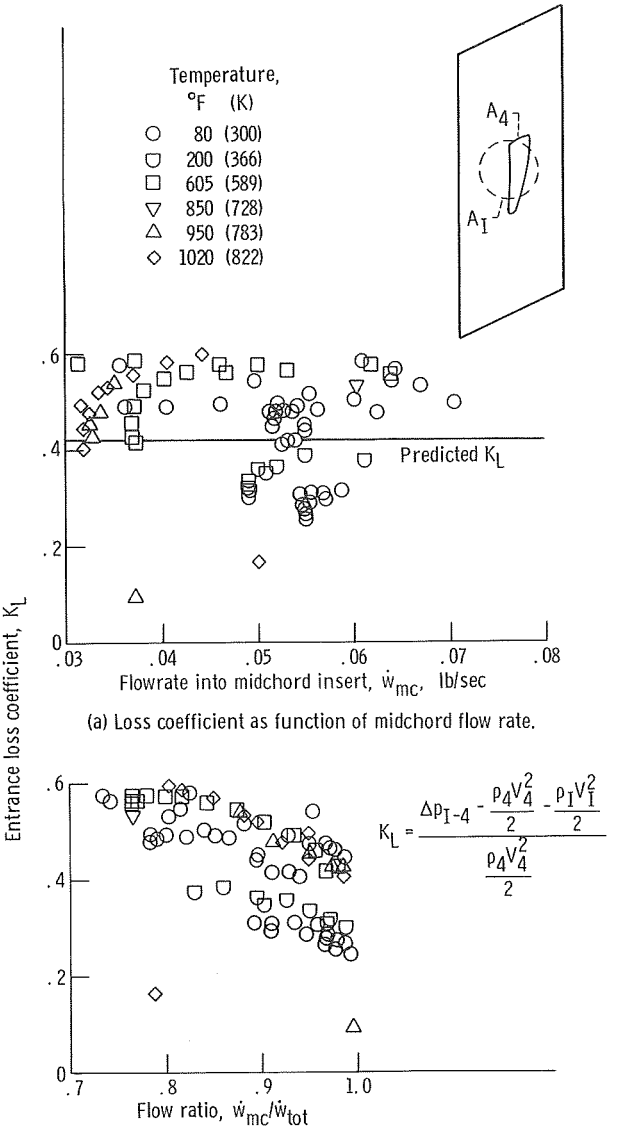

(a) Loss coefficient as function of midchord flow rate.

(b) Loss coefficient as function of total midchord flow ratio.

Figure 11. - Entrance loss coefficient to midchord impingement tube.

pressure in the tip plenum chamber p_1' were nearly the same, and, since p_1' was not recorded on some of the runs, the entrance loss coefficient was calculated based on the difference in total pressure between the inlet supply tube p_I and the midchord supply tube inlet p_4. Figure 11 shows this entrance loss coefficient plotted as a function of flow rate into the midchord supply tube. Also shown on the figure is the value of K_L that would be predicted for the area ratio $A_I/A_4 = 0.31$, that is, $K_L = 0.42$ (ref. 8).

Most of the data shown in figure 11(a) lie above the predicted K_L. The 80° and 200° F (300 and 366 K) data, which fall below the predicted line, were run after the high temperature data were taken. It is believed that something physically changed within the vane during that period which caused these values to be so much different from the others. For example, the pressure measured at p_4 is strongly influenced by its location; thus, if this tube moved, the results should be different. In the vane, although the contraction area ratio is 0.31, the geometry is far from conventional. The sketch in figure 11 shows the relation of the inlet supply tube area A_I to the area of midchord supply tube entrance A_4. Therefore, it is not unreasonable to expect that the measured loss coefficient would be different from the predicted value. The average K_L, not including the low 80° and 200° F (300 and 366 K) data, is about 0.5.

The data shown on figure 11(b) indicate an attempt to correlate the loss coefficient with the ratio of the flow entering the midchord supply tube to the total flow entering the vane. Figure 11(b) shows K_L plotted as a function of this ratio and a definite trend is indicated. As the flow ratio increases, that is, as more of the air flows directly from the inlet tube into the midchord supply tube, the loss coefficient tends more toward the predicted value of 0.42. Thus, the loss coefficient appears to be a function of the amount of air diverted into the leading-edge passage.

Midchord supply tube. - The experimental pressure-drop parameter for the midchord supply tube is shown in figure 12. The pressure-drop parameter $(\rho \Delta p_{fr})_{4-6}$, is plotted against the supply tube inlet flow rate. The density used in the pressure-drop parameter was based on a pressure equal to the average of p_4 and p_6. The frictional pressure drop was obtained from equations (5) or (6). Predicted values of the frictional pressure-drop parameter are shown for comparison in figure 12 for temperatures of 80° and 1000° F (300 and 811 K). The predicted values were obtained by using equation (11) for turbulent flow in pipes. As was the case for the leading-edge exit passage, the difference occurs since the density, flow area, and velocity were assumed constant in the derivation of equation (11). The use of arithmetic averages of the parameters in equation (11) only approximates the result which would have been obtained by integration of equation (5) with variable density, flow area, and velocity along the midchord passage. A theoretical method for predicting the midchord supply tube pressure profile which does not depend on the limiting assumptions of constant density, flow area, and velocity is described in the next section.

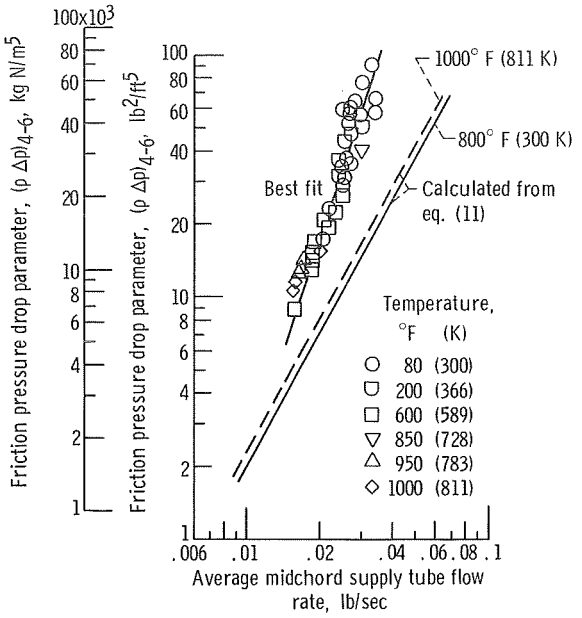

Figure 12. - Friction pressure drop parameter for midchord supply tube as a function of average midchord supply tube flow rate.

Theoretical calculation of pressure change in midchord region. - Theoretical calculations similar to those already described for the leading-edge region were also made for the midchord region. The static-pressure changes in the midchord supply tube were calculated using equation (14d), and the static-pressure profiles in the suction- and pressure-side passages were calculated with equation (14b). The same assumptions were made for the midchord supply tube as for the leading-edge impingement tube with the exception that a 16-percent linear decrease in cross-sectional flow area was considered from tip to hub. The flow remaining in the midchord supply tube at a given distance from the passage entrance was assumed proportional to the total area of the impingement holes from that point to the bottom of the supply tube. The assumptions for the midchord suction- and pressure-side passages were the same as for the leading-edge exit passage, except that the cross-sectional areas of the midchord suction- and pressure-side passages were assumed constant and the flows in the passages at a given distance from the passage entrances were assumed to be proportional to the impingement hole area upstream of that point.

The theoretical and experimental results for the midchord region are given in table I and figure 9. As was the case for the leading-edge impingement tube, the static pressure in the midchord supply tube increases in the flow direction. The calculated ratios of p_6/p_4 vary from 1.09 to 1.10, but the measured values range from 1.05 to 1.10. The static-pressure profiles in the midchord supply tube are predicted reason-

ably well with the largest error in predicted pressure at the hub for the case of high flow at ambient temperature. There are several reasons that could account for the difference between the theoretical predictions and experimental data for the midchord supply tube. First, equation (14d) was derived for fully developed flow, whereas the flow in the entrance region at p_4 is not fully developed. Moreover, a small error in the spanwise location of p_4 will have a considerable effect on the experimental pressure ratio p_6/p_4. Finally, the variation of supply tube impingement hole discharge coefficient with internal Mach number and external flow variation in the suction- and pressure-side passages of the midchord region were not accounted for in the theoretical analysis because of insufficient data.

The experimental results for the midchord pressure-side passage are predicted reasonably well by theory. The total flow rate in the pressure-side passage was calculated with equation (19). For the four typical runs presented in table I, the predicted static-pressure drop ratio p_{10}/p_8 for the midchord pressure-side passage varies from 0.97 at the elevated temperature runs to 0.98 for the ambient temperature run. Experimental values ranged from 0.96 to 0.95 for these runs.

The flow rate in the suction-side passage was also determined using equation (19). The theoretical predictions for the suction-side passage, however, are generally poorer with predicted pressure ratios p_4/p_7 of 0.95 and experimental values of 0.99. A possible explanation for the poor agreement on the suction side is an abnormally high-pressure reading at p_9, probably due to direct impingement of cooling air flow on the pressure tap from the midchord supply tube. Moreover, the predicted pressure drop in the midchord pressure-side passage is always greater than the experimental pressure drop, whereas the predicted pressure drop in the midchord suction-side passage is always less than the experimental pressure drop. Therefore, it is also possible that some of the error might be attributed to inaccurate values of the split in total midchord region flow between the pressure- and suction-side passages.

Trailing-Edge Region

Film-cooling slots. - The suction and pressure surface film-cooling slots are shown schematically in figure 13. The air makes its way through the midchord supply tube impingement holes and between the supply tube and outer walls of the vane. Then the air either exits through one of the film-cooling slots or through the split trailing edge. The film-cooling slots consist of a row of small oblong holes feeding much larger slots; the pressure-side slot runs continuously from hub to tip and the suction side has eight oblong slots from hub to tip. Compressible discharge coefficients (eq. (21)) were calculated and plotted as a function of the pressure-drop parameter $\rho_{coll}\overline{\Delta p}$ for each of

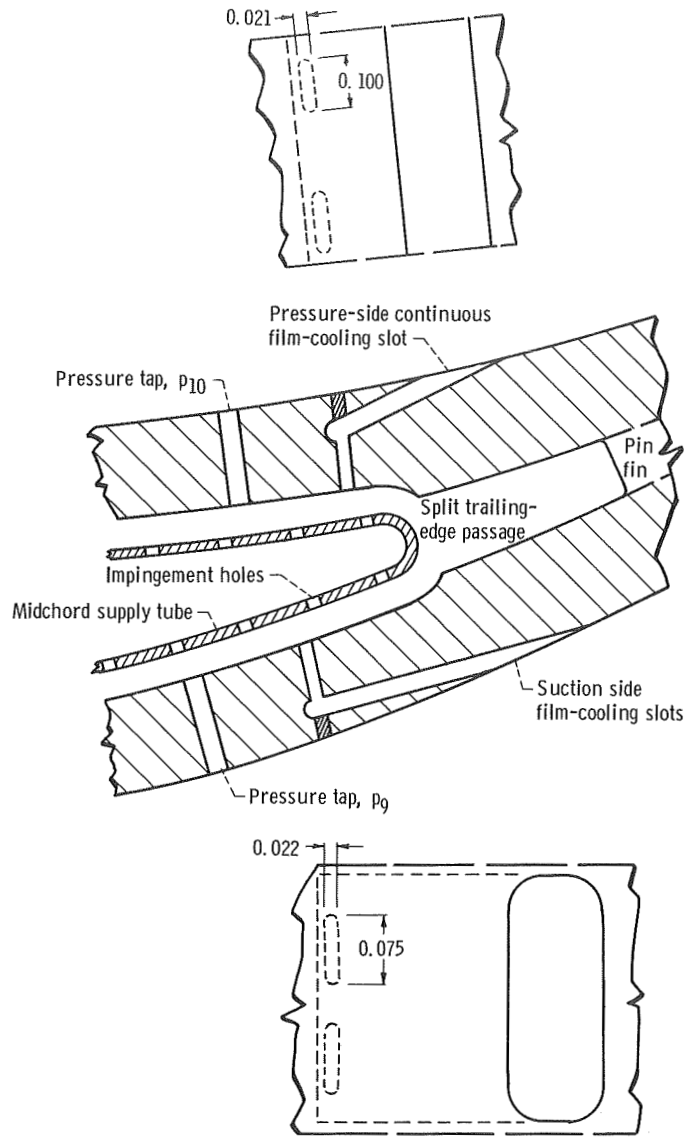

Figure 13. - Film-cooling slot configuration.

the slots. The results are shown in figure 14. The data from the suction-side slot are correlated by the line

$$C_{D,\,suc} = 0.180(\rho_{coll,\,suc}\,\overline{\Delta p})^{0.12}$$

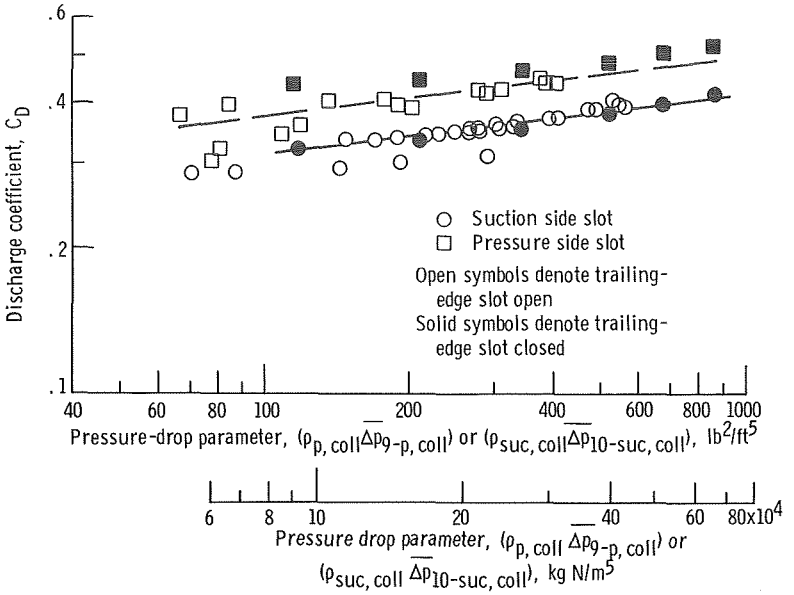

Figure 14. - Film-cooling slot discharge coefficients as a function of pressure drop parameter.

On the other hand, the pressure-side data were correlated by

$$C_{D,p} = 0.266(\rho_{coll,p}\overline{\Delta p})^{0.12}$$

The magnitude of the coefficients is much lower than similar thick-plate discharge coefficients. Additional turning and expansion losses cause the lower coefficients in this case.

Split trailing edge. - The split trailing-edge pin-fin configuration is shown in the sketch in figure 15. There are four rows of staggered, oblong pin fins, with the long dimension set perpendicular to the direction of the air flow and one row of cylindrical pin fins. The first attempt to correlate the pressure-drop data for this passage is shown in figure 15. Here, the pressure-drop parameter $(\rho\ \Delta\bar{p})_{11\text{-te}}$ is plotted as a function of tailing-edge flow rate. The pressure at the passage inlet $\bar{p}_{11}$ is calculated by using Simpson's rule. The measured pressure in the trailing-edge collector subtracted from $\bar{p}_{11}$ is the pressure drop. The density was based on the average of $\bar{p}_{11}$ and the collector pressure. The data correlated reasonably well with the empirical curve:

$$\dot{w}_{te} = 0.00184(\rho\ \Delta\bar{p})^{0.5}_{11\text{-te}}$$

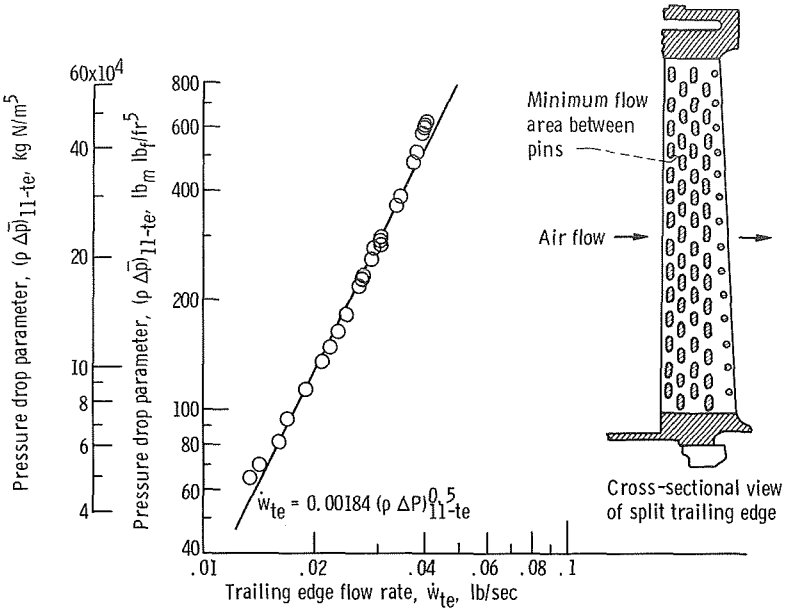

Figure 15. - Pressure-drop parameter for split trailing edge as function of trailing-edge flow rate.

To find the pin-fin friction pressure drop through the split trailing edge, the exit loss from the trailing-edge exit to the collector was calculated using equation (2). The static pressure at the trailing-edge exit was then calculated from the total pressure at that point. Finally, the friction pressure drop was found by subtracting the momentum pressure drop from the static-pressure drop. Then, the friction factor was calculated from equation (12). The results are plotted in figure 16 as a function of Reynolds number (based on average minimum flow area between pins in the last two pin rows, and on equivalent pin diameter). The equivalent pin diameter was found such that the cross-sectional area of the equivalent pins and the actual pins were the same. The average minimum flow area occurs between adjacent pin rows as shown in the sketch on figure 15. Shown on figure 16 is the range of data obtained by Theoclitus (ref. 5) for in-line pin-fins. Although the maximum Reynolds number investigated by Theoclitus was about 7000, the friction factors obtained in this study were of the same magnitude.

Jakob (ref. 6) correlated data obtained from various staggered pin-fin configurations with the empirical relation given by equation (13). The upper line in figure 16 was calculated using this correlation with an equivalent pin diameter. The lower line was calculated using the Jakob equation with average flow hydraulic diameter replacing the equivalent pin diameter. The square symbols on the figure correspond to the experimental data calculated also using the average flow hydraulic diameter. The agreement between predicted and experimental results is somewhat improved when the minimum flow area hydraulic diameter is used in the Jakob equation.

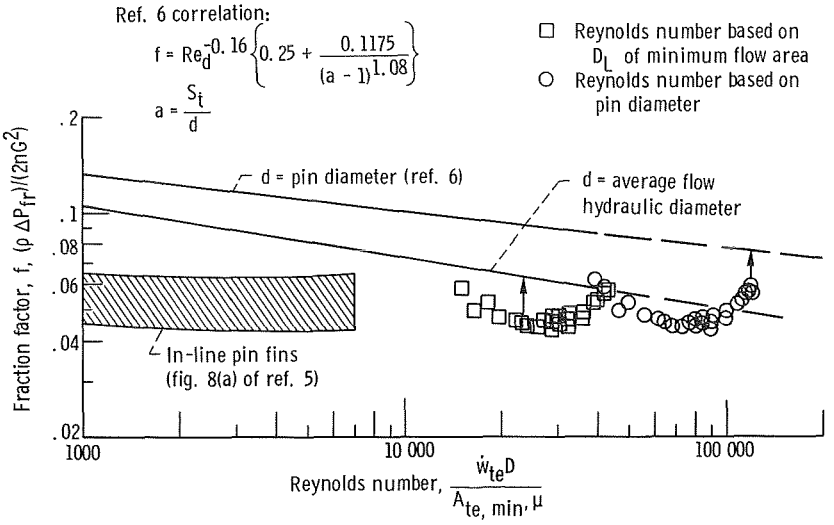

Figure 16. - Trailing-edge friction factor as function of Reynolds number.

Application of Results to Engine and Static Cascade

Leading edge. - As mentioned earlier, the flow and pressure results obtained in this study will be used in future heat-transfer tests on this vane configuration in a static cascade facility and in a turbine development engine facility. In either the static cascade or the engine, the coolant inlet flow rate, temperature, and pressure will be measured (or will be found from other measurements). Also, the pressure to which the leading-edge exit passage exhausts will be measured. Thus, the ordinate of figure 8 is completely known: density evaluated at the average pressure from inlet to leading-edge outlet and pressure drop found from the difference between the inlet and outlet pressures. As discussed previously, the momentum change caused by an increase in the coolant temperature during engine and cascade tests must be subtracted from the measured pressure drop before using figure 8. The flow rate through the leading edge may then be read directly from figure 8.

Next, equation (2) may be solved iteratively to find the total pressure at the end of the leading-edge exit passage (see fig. 6). Since the leading-edge flow rate is known, the static pressure at the end of the leading-edge exit passage can be calculated. Then, equation (6) may be used with figure 7 to calculate the pressure at the entrance to the leading-edge exit passage. Theoretical predictions based on equation (14b) have indicated that the pressure distribution between the leading-edge exit passage inlet and outlet is approximately parabolic in shape with a maximum (i.e., $dp/dx = 0$) at the passage inlet. If this pressure profile is assumed, equation (14b) may be used to calculate the mass flow-rate distribution in the exit passage. This passage flow-rate dis-

tribution will then define the flow distribution in the leading-edge impingement tube.

Midchord supply tube. - The flow rate into the midchord supply tube will simply be the difference between the flow rate entering the vane and the leading-edge flow rate. Equation (1) will be used to calculate the total pressure at the inlet to the midchord supply tube from the total pressure in the inlet supply tube. The static pressure at the inlet to the midchord supply tube is readily calculated since flow rate is known. The entrance loss coefficient K_L was (fig. 11) about 0.5. Next, equation (14d) must be solved to find the static-pressure distribution or the flow distribution within the midchord supply tube; since they are not independent, a flow-rate or pressure distribution must be assumed, and the other variable may then be calculated. In the upcoming engine and static cascade tests, there will be no pressure measurements made within the midchord supply tube. If a flow distribution within the midchord supply tube is assumed such that the local flow at a given distance from the tube inlet is proportional to the flow area through the porous wall from that point to the end of the passage, then the measured static-pressure profile could be predicted from equation (14d) with reasonable accuracy. Thus, the pressure distributions within the midchord supply tube can be calculated using this method.

Midchord chordwise flow passages. - In the midchord chordwise flow passages, pressures are to be measured at locations 7 to 10 and 7'' to 10'' in the engine and static cascade tests. The method described in the section Midchord Chordwise Flow Rate Calculation may be used to calculate the flow rate along these two passages. The average pressure inside the midchord supply tube can be found from the distribution calculated using equation (14d). The chordwise passage average inlet and outlet pressures may be found by averaging the readings at locations 7 and 7'', 8 and 8'', 9 and 9'', and 10 and 10''. Equations (17) to (19) may then be used to calculate $\dot{w}_{suc,N}$ and $\dot{w}_{p,N}$.

Flow rate through film-cooling slots and split trailing edge. - All air that enters the midchord supply tube must discharge through one of the two film-cooling slots or through the split trailing-edge passage. The external pressure distribution or discharge pressures for each of these passages will be calculated for the engine and static cascade tests from the hot gas flow rate, vane geometry, etc. Then the abscissa of figure 14 may be determined completely, and a discharge coefficient read directly from the line in figure 14. Equation (20) will be used to calculate the ideal flow rate through each of the film-cooling slots and the actual flow rate will be found from equation (21). In the split trailing edge, pressures will be measured at locations 11 and 11'' (fig. 4) and thus the ordinate of figure 15 may be calculated. The density will be based on the average of p_{11} and p_{te}. All momentum terms must be subtracted before figure 15 can be used to determine the actual flow rate through the split trailing edge. These actual flow rates should then be normalized so that the sum of the flow rates leaving the three passages equals the flow rate entering the midchord supply tube.

Overall Comparisons

Comparisons of measured and calculated flow distributions are presented in table II for two cooling air temperatures and selected runs with low, medium, and high total flow rates. For the high temperature cases, only total and leading-edge flows were measured; the difference between these measurements is compared with the sum of the

TABLE II. - COMPARISON OF MEASURED AND PREDICTED FLOW RATES

(a) Low flow rate run; inlet coolant flow rate, 0.032 pound per second (14.6 g/sec)

Region	Temperature, °F (K)							
	80 (300)				1000 (811)			
	Flow rate							
	Measured		Predicted		Measured		Predicted	
	lb/sec	g/sec	lb/sec	g/sec	lb/sec	g/sec	lb/sec	g/sec
1. Leading edge	0.0088	4.0	0.0090	4.1	0.0005	0.2	------	----
2. Suction side slot	.0034	1.6	.0036	1.6	} .0318	14.4	0.0039	1.8
3. Pressure side slot	.0058	2.6	.0055	2.5			.0058	2.6
4. Trailing edge slot	.0161	7.3	.0151	6.9			.0147	6.7
5. Suction side passage[a]	-----	----	.0123	5.6	-----	----	.0182	11.1
6. Pressure side passage[a]	-----	----	.0091	4.1	-----	----	.0138	8.3
Total (1 + 2 + 3 + 4)	.0341	15.5	.0332	15.1	.0323	14.6	.0244	11.1
(b) Medium flow rate run, inlet coolant flow rate, 0.050 pound per second (22.7 g/sec)								
1. Leading edge	0.0130	5.9	0.0130	5.9	0.0091	4.1	0.0090	4.1
2. Suction side slot	.0066	3.0	.0068	3.1	} .0405	18.4	.0056	2.5
3. Pressure side slot	.0027	1.2	.0042	1.9			.0083	3.8
4. Trailing edge slot	.0275	12.5	.0253	11.5			.0192	8.7
5. Suction side passage[a]	-----	----	.0236	10.7	-----	----	.0251	11.4
6. Pressure side passage[a]			.0164	7.4	-----	----	.0191	8.7
Total (1 + 2 + 3 + 4)	.0498	22.6	.0493	22.4	.0496	22.5	.0421	19.1
(c) High flow rate run, inlet coolant flow rate, 0.063 pound per second (28.6 g/sec)								
1. Leading edge	0.0171	7.8	0.0175	8.0	0.0135	6.1	0.0135	6.1
2. Suction side slot	.0063	2.9	.0073	3.3	} .0498	22.6	.0072	3.3
3. Pressure side slot	.0109	4.9	.0111	5.0			.0105	4.8
4. Trailing edge slot	.0307	13.9	.0279	12.7			.0233	10.6
5. Suction side passage[a]	-----	----	.0217	9.8	-----	----	.0189	8.6
6. Pressure side passage[a]	-----	----	.0163	7.4	-----	----	.0144	6.5
Total (1 + 2 + 3 + 4)	.0650	29.5	.0638	29.0	.0633	28.7	.0545	24.8

[a]Suction side and pressure side passage flow rates have been normalized by use of eq. (19). These flow rates were not measured experimentally and, therefore, the predicted values are presented for information only.

calculated flows through the suction- and pressure-surface slots and the split trailing edge. The predicted leading-edge flow rates were obtained from figure 8. The midchord suction- and pressure-side passage flow rates were predicted using equations (14). The predicted flow rates through the film cooling slots were obtained by using figure 14 and equations (20) and (21). Finally the predicted flow rate through the trailing-edge passage was obtained by using figure 15. This comparison indicates excellent agreement for the low temperature runs, as expected, since the data for the trailing-edge slots and film-cooling slots were correlated for the low temperature test. For the high temperature tests the agreement is good for the leading-edge passage, but not nearly as good for the others. As mentioned in the previous section, these flow rates should be normalized to yield more realistic values.

For one run, measured total flow rate and measured inlet and outlet pressures were used to calculate exit flow rates. One calculation was made by use of a computer program, and the other by use of the correlations obtained from the experimental data reported herein. The results are as follows:

	Leading edge	Suction slot	Pressure slot	Trailing edge
	Exit flow rate, lb/sec (kg/sec)			
Computer	0.0190 (0.0086)	0.0068 (0.0031)	0.0089 (0.0040)	0.0279 (0.0127)
Correlations	.0188 (0.0085)	.0072 (0.0033)	.0077 (0.0035)	.0282 (0.0128)

A three-dimensional heat-transfer computer program was used to predict the variation in vane metal temperatures which would be expected between calculations based on the actual vane flow distribution and those based on vane flow distributions obtained from the correlations presented in this report. The results of these calculations indicated that the maximum error in calculated vane metal temperature associated with the use of the vane flow distributions presented in this report is $\pm 40^{\circ}$ F (22.2 K).

SUMMARY OF RESULTS

An experimental flow study of a complex air-cooled vane was completed, and the experimental data were compared with predictions for the leading-edge, midchord, and trailing-edge regions of the vane. The results are summarized herein for each of the three regions.

Leading-Edge

The overall pressure drop in the leading-edge region could be correlated with leading-edge flow rate over the range of interest. The experimental pressure-drop data for the leading-edge exit passage were considerably larger than those calculated with an incompressible turbulent flow equation. The one-dimensional momentum analysis adequately predicted experimental leading-edge exit passage pressure drops over a representative range of flow rates and temperatures.

Midchord

The experimental midchord inlet pressure-loss coefficients values (K_L approximately 0.5) were somewhat higher than those predicted for incompressible flow loss for concentric tubes with the same area ratio ($K_L = 0.42$). As was the case for the leading-edge exit passage, the frictional pressure drop in the midchord supply tube was larger than that predicted with incompressible turbulent flow equations for a smooth tube. The experimental friction pressure drop parameter, however, correlated reasonably well with the average flow rate in the midchord supply tube.

A modified one-dimensional momentum analysis for determining the static pressure rise in a passage with flow ejection gave reasonably good agreement with experimental results for the midchord supply tube. Also, the one-dimensional momentum analysis for the case of flow injection into a passage predicted the static pressure drop in the midchord suction and pressure passages fairly well.

Trailing Edge

The pressure drops through the suction and pressure surface film-cooling slots in the trailing-edge region were correlated with compressible discharge coefficients. The pressure drop parameter for the split trailing-edge correlated fairly well with the square of the trailing edge flow rate. Although the experimental friction factors for the split trailing edge were beyond the Reynolds number range of available empirical correlations, the data showed qualitative agreement with the correlations.

It is estimated that the errors in vane flow-rate distributions predicted using the experimental correlations presented in this report will result in a maximum error of $\pm 40^{\circ}$ F (22.2 K) in calculated vane metal temperatures.

In conclusion, computational techniques have been developed that will be used, with reasonable confidence, to predict local values of flow rate and pressure.

Lewis Research Center,
National Aeronautics and Space Administration,
Cleveland, Ohio, March 4, 1970,
720-03.

APPENDIX A

SYMBOLS

The following symbols, with consistent units, are used:

A	cross-sectional area of flow passage
a	pin-fin transverse spacing to pin diameter ratio, S_t/d
a_v	acoustic velocity
C_D	discharge coefficient
D_h	hydraulic diameter of flow passage
d	diameter
F	frictional force
f	friction factor
G	specific mass flow rate, $\dot{w}/A$
g	acceleration due to gravity
K_L	entrance loss coefficient
L	length of passage
M	Mach number at passage inlet
N	number of holes
n	number of rows of pin fins, pressure tap location
P	total pressure
p	static pressure
R	gas constant
Re	Reynolds number, $\frac{\dot{w}}{A}\frac{D_h}{\mu}$
r	radius to element measured in plane of rotation
S_t	transverse fin spacing
T	temperature
V	velocity
$\dot{w}$	coolant flow rate
x	distance from passage inlet

z	height
β	angle between velocity vector and direction of increasing r
γ	ratio of specific heats
ϵ	ratio of upstream area to downstream area
μ	viscosity
ξ	dimensionless length
ρ	density
ω	angular velocity

Subscripts:

av	average
coll	collector
d	pin diameter
e	bottom of leading edge impingement tube
fr	friction
i	insert
id	ideal
in	inlet
le	leading edge
m	momentum
meas	measured
mc	midchord
min	minimum
N	normalized
out	outlet
p	pressure side
s	static
suc	suction side
te	trailing edge
x	exit

I, 1, 1', 2, 3,
4, 5, 6, 7, 7',
7'', 8, 8', 8'',
9, 9', 9'', 10,
10', 10'', 11,
11', 11'', 14

locations of pressure taps

APPENDIX B

DERIVATION OF PRESSURE CHANGE EQUATION FOR FLOW EJECTION THROUGH POROUS WALL

The basic equation for flow in a passage with ejection through a porous wall is derived based on the flow model shown in figure 5. This model differs from that of reference 7 with respect to the direction of the momentum vector leaving the control flow surface. In this derivation it is assumed that the ejected flow leaves the control surface with the same velocity vector as the mainstream. The exiting flow is then turned first in the boundary layer and then in the porous wall before leaving the flow passage through the porous wall.

The net sum of the forces acting on the control surface can be equated to the change in momentum of the fluid flowing through the control surface. The sum of the pressure forces is

$$p_{in}A - (p_{in} + dp_{in})(A + dA) + \left(p_{in} + \frac{dp_{in}}{2}\right)dA$$

where $p_{in} + (dp_{in}/2)$ is the approximation for pressure at the passage wall surface. When second order terms are neglected, the expression for the net pressure force on the control surface is $-A\ dp_{in}$. The frictional force acts in a direction opposite to the flow and is given by

$$dF = \frac{4f\ dx\ \rho V^2 A}{2D_h}$$

The increase in momentum across the control surface is

$$(\dot{w} - d\dot{w})(V + dV) + d\dot{w}\left(V + \frac{dV}{2}\right) - \dot{w}V$$

Neglecting second-order terms results in a net increase in momentum $\dot{w}\ dV$. Equating the pressure and frictional forces to the increase in momentum gives

$$-A\ dp_{in} - \frac{4f\ dx\ \rho V^2 A}{2D_h} = \dot{w}\ dV$$

With the use of the continuity equation and the equation of state for a perfect gas, the final equation for pressure in a passage with ejection through a porous wall is readily obtained

$$\left[1 - \frac{RT}{p_{in}^2}\left(\frac{\dot{w}}{A}\right)^2\right]\frac{dp_{in}}{dx} = -\frac{RT}{p_{in}}\frac{\dot{w}}{A}\frac{d\frac{\dot{w}}{A}}{dx} - \frac{R}{p_{in}}\left(\frac{\dot{w}}{A}\right)^2\left(\frac{dT}{dx} + \frac{4fT}{2D_h}\right)$$

For the case of flow ejection from a porous passage, the solution of the above equation predicts a decrease in total pressure, whereas the solution of equation (14b) predicts an increase in total pressure. If it is assumed that the flow model is correct based on experimental results from the vane flow tests, it is suggested that the use of equation (14b) be restricted to the case of flow injection through a porous wall.

REFERENCES

1. Rohde, John E.; Richards, Hadley T.; and Metger, George W.: Discharge Coefficients for Thick Plate Orifices with Approach Flow Perpendicular and Inclined to the Orifice Axis. NASA TN D-5467, 1969.

2. Calvert, Howard F.; Cochran, Reeves P.; Dengler, Robert P.; Hickel, Robert O.; Norris, James W.: Turbine Cooling Research Facility. NASA TM X-1927, 1970.

3. Vennard, John K.: Elementary Fluid Mechanics. Third ed., John Wiley & Sons, Inc., 1954.

4. McAdams, William H.: Heat Transmission. Third ed., McGraw-Hill Book Co., Inc., 1954.

5. Theoclitus, G.: Heat-Transfer and Flow-Friction Characteristics of Nine Pin-Fin Surfaces. J. Heat Transfer, vol. 88, no. 4, Nov. 1966, pp. 383-390.

6. Jakob, Max: Heat Transfer and Flow Resistance in Cross Flow of Gases Over Tube Banks. Discussion. Trans. ASME, vol. 60, no. 4, May 1938, pp. 384-386.

7. Eckert, E. R. G.; Livingood, John N. B.; and Prasse, Ernst I.: One-Dimensional Calculation of Flow in a Rotating Passage with Ejection Through a Porous Wall. NACA TN 3408, 1955.

8. Anon.: Flow of Fluids through Valves, Fittings, and Pipe. Tech. Paper 410, Crane Co., 1965.

NASA-Langley, 1970 —— 1 E-5558

NATIONAL AERONAUTICS AND SPACE ADMINISTRATION
WASHINGTON, D. C. 20546

OFFICIAL BUSINESS

FIRST CLASS MAIL

POSTAGE AND FEES PAID
NATIONAL AERONAUTICS AND
SPACE ADMINISTRATION

POSTMASTER: If Undeliverable (Section 158 Postal Manual) Do Not Return

"The aeronautical and space activities of the United States shall be conducted so as to contribute . . . to the expansion of human knowledge of phenomena in the atmosphere and space. The Administration shall provide for the widest practicable and appropriate dissemination of information concerning its activities and the results thereof."

—NATIONAL AERONAUTICS AND SPACE ACT OF 1958

NASA SCIENTIFIC AND TECHNICAL PUBLICATIONS

TECHNICAL REPORTS: Scientific and technical information considered important, complete, and a lasting contribution to existing knowledge.

TECHNICAL NOTES: Information less broad in scope but nevertheless of importance as a contribution to existing knowledge.

TECHNICAL MEMORANDUMS: Information receiving limited distribution because of preliminary data, security classification, or other reasons.

CONTRACTOR REPORTS: Scientific and technical information generated under a NASA contract or grant and considered an important contribution to existing knowledge.

TECHNICAL TRANSLATIONS: Information published in a foreign language considered to merit NASA distribution in English.

SPECIAL PUBLICATIONS: Information derived from or of value to NASA activities. Publications include conference proceedings, monographs, data compilations, handbooks, sourcebooks, and special bibliographies.

TECHNOLOGY UTILIZATION PUBLICATIONS: Information on technology used by NASA that may be of particular interest in commercial and other non-aerospace applications. Publications include Tech Briefs, Technology Utilization Reports and Notes, and Technology Surveys.

Details on the availability of these publications may be obtained from:

SCIENTIFIC AND TECHNICAL INFORMATION DIVISION

NATIONAL AERONAUTICS AND SPACE ADMINISTRATION

Washington, D.C. 20546